Melillo, A.; García-Vallés, C.; Ferrer Ribera, RB.; Alvaro Rodríguez, MM.; Navalón Oltra, S.; García Gómez, H. (2021). Bifunctional metal-organic frameworks for the hydrogenation of nitrophenol using methanol as the hydrogen source. Organic & Biomolecular Chemistry. 19(4):794-800. https://doi.org/10.1039/d0ob01686a

ARTICLE

Bifunctional metal-organic frameworks for hydrogenation of nitrophenol using methanol as hydrogen source

Received 00th January 20xx,
Accepted 00th January 20xx

DOI: 10.1039/x0xx00000x

Arianna Melillo,[a] Cristina García-Vallés,[a] Belén Ferrer,[a,*] Mercedes Álvaro,[a] Sergio Navalón, [a,*] Hermenegildo García[a,b,c,*]

This work reports the reduction of 4-nitrophenol to 4-aminophenol using UiO-66(Zr) as bifunctional, photocatalyst and hydrogenation, catalyst using methanol as hydrogen source. In particular, a series of UiO-66(Zr)-X (X: NH_2, NO_2 and H) and MIL-125(Ti)-NH_2 have been screened as bifunctional catalysts for this process. UiO-66(Zr)-NH_2 was found the most active material to promote the light-assisted nitro hydrogenation under both UV-Vis and simulated sunlight irradiation. The tandem reaction occurs via hydrogen generation from water/methanol mixture in a first step and, then, reduction of the 4-nitrophenol to 4-aminophenol. UiO-66(Zr)-NH_2 acts as a truly heterogeneous catalyst and can be reused several times without significant loss of activity, maintaining its crystallinity. This work shows the possibility of using MOFs as solar-driven bifunctional catalysts to promote hydrogenation of organic compounds using methanol as hydrogen source.

Introduction

Metal-organic frameworks (MOFs) in which the lattice is defined by metal nodes held in place by rigid organic linkers forming a crystalline, porous solid are among the preferred hybrid organic-inorganic catalysts.[1-5] MOFs offer a wide range of active sites including exchangeable coordination positions around the metal ions, acid or basic substituents on the organic linker or active guests incorporated within the empty voids.[6-12] In addition, MOFs may exhibit photoresponse and they are among the most active photocatalysts for aerobic oxidations,[13-17] overall water splitting[18-21] and CO_2 reduction[22-26] among other reactions.[27]

The presence of more than one active site renders MOFs very suited hybrid catalysts to promote tandem reactions in which more than elementary conversion.[28-31] Among the numerous examples of MOFs as catalysts for tandem reactions, one type that is growing in interest is those reactions combining a light-assisted transformation with a dark catalytic reaction.[32-33] One photocatalytic reaction that is attracting considerable interest due the possible role of hydrogen as energy vector and the efficiency of MOFs in comparison to other semiconductors, is the photocatalytic hydrogen generation.

In this context, it occurred to us that the ability of MOFs to generate in situ hydrogen could be combined with the use of hydrogen in a hydrogenation reaction, developing a so far unreported tandem reaction. The obvious advantage of this tandem photocatalytic H_2 generation-catalytic hydrogenation would be that no H_2 gas is needed and the process is easily controlled by on-off switching of the light.

In the present manuscript, the concept of in situ photocatalytic H_2 generation to carry out catalytic hydrogenations has been proved using a series of five MOFs with MIL-125(Ti) and UiO-66(Zr) structure that are among the most widely studied photocatalysts for H_2 generation. The photocatalytic activity of MIL-125(Ti)-NH_2, UiO-66(Zr)-H and UiO-66(Zr)-NH_2 can be found in the literature. The light-assisted H_2 generation is combined with the presence of frustrated Lewis acid-base pairs in the MOFs to perform nitro aromatic hydrogenation to aniline that is a process of large industrial importance in the production of polyurethane monomers. It will be shown that UiO-66(Zr)-NH_2 is a reusable and stable heterogeneous catalysts for this light-assisted tandem reaction.

Experimental section

Materials

Detailed information about the manufacturer and purity of all reagents and solvents employed in this work: Zirconium tetrachloride: Sigma Aldrich > 99.5% trace metals basis; Terephthalic acid: Sigma Aldrich 98%; N, N'-Dimethylformamide: Sharlab; Methanol: Sharlab; 2- amino terephthalic acid: Sigma Aldrich; 2-nitro terephthalic acid: Sigma Aldrich; Titanium isopropoxide: Sigma Aldrich > 97%; 4-nitrophenol: Sigma Aldrich > 99.9%.

Catalyst preparation

[a.] *Departamento de Química, Universitat Politècnica de València, Camino de Vera s/n, Valencia 46022, Spain.*
[b.] *Instituto Universitario de Tecnología Química, CSIC-UPV, Universitat Politècnica de València, Av. de los Naranjos, Valencia 46022, Spain.*
[c.] *Address here.*

† Footnotes relating to the title and/or authors should appear here.

Electronic Supplementary Information (ESI) available: [details of any supplementary information available should be included here]. See DOI: 10.1039/x0xx00000x

The list of MOFs employed in this study include UiO-66(Zr)-X (X: NH_2, NO_2 and H) and MIL-125(Ti)-NH_2 and have been prepared following previously reported procedures. [20,34-35] Supplementary information collects the detailed procedure for the solvothermal preparation of each solid.

Characterization of the materials.

Powder X-ray diffraction (PXRD) patterns were recorded on a Philips XPert diffractometer equipped with a graphite monochromator (40 kV and 45 mA) employing Ni filtered Cu Kα radiation. Isothermal N_2 adsorption measurements have been carried out at 77 K using a Micromeritics ASAP 2010 apparatus. The metal content of each MOF material was determined by ICP-AES analysis after digesting the solids in concentrated nitric acid at 80 ºC for 24 h. ATR-FTIR spectra of MOFs were measured with a Bruker Tensor 27 instrument. Previously to ATR-FTIR measurements the MOF samples were dried in an oven at 100 °C for 24 h to remove physisorbed water

Photocatalytic and thermocatalytic experiments

The light-assisted catalytic activity of UiO-66(Zr)-X (X: NO_2, NH_2 or H) and MIL-125(Ti)-NH_2 was evaluated for the reduction of 4-nitrophenol (NP) to 4-aminophenol (AP). Briefly, the required catalyst amount (i.e. 5 mg) was introduced into a quartz reactor with a total volume of 51 mL containing a pressure gauge on the outlet and one gas inlet, which is shown in Figure S1. Then, a solution of 4-nitrophenol (0.02 mmol) dissolved in a mixture of water (1.25 mL) and methanol (1.25 mL) was added and the suspension submitted to ultrasounds for 20 min. Subsequently, the system was purged with Ar for 15 min. The reaction was irradiated by means of an optical fiber with the output of a Xe lamp (150 W) equipped or not with a 1.5 AM to simulate sunlight. The course of the reaction was followed by UV-vis spectroscopy (200-800 nm) analyzing diluted reaction aliquots (0.1 mL) in acetonitrile (2.9 mL). Prior to record the UV-vis spectra the suspension was filtered using a Nylon filter (0.2 μm).

Photocatalytic hydrogen generation using the MOF samples was evaluated using the sample procedure described for the photocatalytic reduction using 5 mg of MOF, but in the absence of 4-nitrophenol. The evolving gases were analyzed from the head space, connecting directly the reactor to an Agilent 490 Micro GC system (Molsieve 5 Å column using Ar as carrier gas) without manual handling. Throughout the experiment the temperature of the system was monitored and the pressure was determined by the manometer adapted to the photoreactor chamber.

Catalytic hydrogenation promoted by MOFs (5 mg) for 4-nitrophenol (0.02 mmol) hydrogenation was performed in water-ethanol solution using hydrogen atmosphere (1 bar) at 50 °C.

Results and discussion

Catalyst preparation

The MOFs under study were prepared by solvothermal synthesis following previous reported procedures. [20, 34-35] Figure 1 (a1 and a2) shows that the experimental PXRD patterns obtained for the UiO66 series MOFs and for MIL-125(Ti)-NH_2 coincide with the simulated ones. PXRD patterns confirm the successful formation of crystalline MIL-125(Ti)-NH_2[36] material as well as that of isostructural UiO-66(Zr)-H, UiO-66(Zr)-NH_2 and UiO-66(Zr)-NO_2 solids (Figure 1 a1 and a2).[37-39] The difference of UIO-66, UiO-66(Zr)-NH_2, UiO-66(Zr)-H and UiO-66(Zr)-NO_2 in the pattern has been marked in Figure S2. It can be observed that the main peak is slightly shifted to the right for UiO-66(Zr)-NH_2 and to the left for UiO-66(Zr)-NO_2. Diffuse reflectance UV-Vis spectroscopy of the series of MOFs under study confirms the bathochromic shift in the absorption spectrum of the parent MIL-125(Ti) and UiO-66(Zr) materials due to the presence in the terephthalate linker of –NH_2 or -NO_2 groups (Figure 1b).[36-39] Tauc plots derived from optical measurements allow estimation of the values of 2.71, 3.11, 2.72 and 2.82 eV for the band gaps of MIL-125(Ti)-NH_2, UiO-66(Zr)-H, UiO-66(Zr)-NH_2 and UiO-66(Zr)-NO_2, respectively. These band gap values are in good agreement with the reported values (Figure S3).[20-21,40]

FT-IR spectroscopy reports on the nature of the different functional groups present on the terephthalate ligand of the MOF samples, by monitoring the characteristic vibrational peaks associated to COO- (1582 and 1391 cm^{-1}), -NH_2 (3482 and 3386 cm^{-1}) and -NO_2 (1500 and 1380 cm^{-1}) (Figures S4-S7).

The BET surface area and pore volumes of the MOFs under study were determined by isothermal N_2 adsorption measurements at 77 K (Table 1 and Figures S8-S11). These values are in general agreement with previous reports, indicating the porosity decrease due to the presence of NH_2 or NO_2 substituents of terephthalate ligand occupying some internal space in comparison to the values of parent UiO-66(Zr)-H. ICP-AES analyses of previously acid-digested MOFs are in good agreement with the theoretical Ti or Zr content, respectively, for the MIL-125(Ti)-NH_2 or UiO-66(Zr)-X materials under study. A summary of the characterization data is provided in Table 1. The morphology of the particles has been studied by HRSEM. Figure S12 shows the HRSEM images and particle size distribution obtained for the MOFs under study. The average particle size values obtained for the different MOFs, summarized in table S1, are in the same range. Therefore, it can be concluded that the particle size will not be a determining factor in the catalytic activity of the MOFs. The morphology of the particles has also been studied by TEM. Figure S13 shows the TEM images of the different MOFs.

Tandem light-assisted H_2 generation-hydrogenation reaction

The activity of the MOFs under study as bifunctional catalysts in the tandem reaction was evaluated for the reduction of 4-nitrophenol to 4-aminophenol using methanol as hydrogen source. The tandem process involves photocatylic H_2 generation from methanol and subsequent hydrogenation of nitro group.

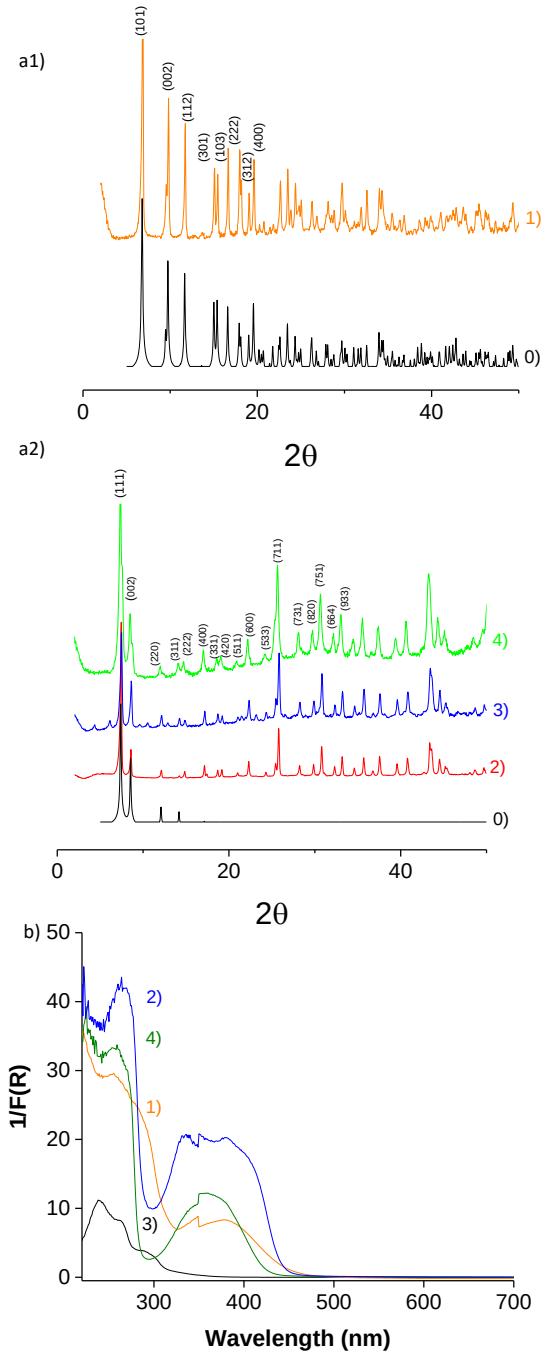

Figure 1. Simulated (0) and experimental PXRD (a1 and a2) and diffuse reflectance UV-Vis spectra (b) of MIL-125(Ti)-NH2 (1), UiO-66(Zr)-NH_2 (2), UiO-66(Zr)-H (3) and UiO-66(Zr)-NO_2 (4).

Table 1. List of MOFs employed as bifunctional catalysts in this work together with some relevant porosity and analytical data.

Entry	Theoretical MOF formula	BET surface area (m^2/g)	Pore volume (cm^3/g)	Theoretical (%) / Experimental metal content (%)
MIL-125(Ti)-NH_2	$Ti_8O_8(OH)_4(C_6H_3C_2O_4NH_2)_6$	1200	0.57	23.0 / 21.7
UiO-66(Zr)-H	$Zr_6O_4(OH)_4(OOC\text{-}C_6H_4\text{-}COO)_6$	1368	0.80	32.8 / 31.6
UiO-66(Zr)-NH_2	$Zr_6O_4(OH)_4(OOC\text{-}C_6H_3NH_2\text{-}COO)_6$	923	0.91	31.2 / 30.9
UiO-66(Zr)-NO_2	$Zr_6O_4(OH)_4(OOC\text{-}C_6H_3NO_2\text{-}COO)_6$	903	0.66	28.2 / 27.4

In the first step, light absorption leads to electron/hole separation in the conduction/valence bands, resulting in H_2 evolution from methanol as sacrificial agent. Four materials, namely, MIL-125(Ti)-NH_2, UiO-66(Zr)-H and UiO-66(Zr)-NH_2 have been reported as photocatalyst for H_2 generation from methanol. The second step, MIL-125(Ti)-NH_2 and UiO-66(Zr)-X in the absence of any metal as hydrogenation catalyst has not been previously disclosed.

Preliminary control experiments reveal that the photocatalytic hydrogen generation from methanol or 4-nitrophenol hydrogenation does not occur in the absence of MOF. An additional control experiment reveals that p-nitrophenol reduction to p-aminophenol does not occur upon MOF irradiation in the absence of methanol. This result agrees with the higher photocatalytic H_2 production using MOFs as photocatalysts in the presence of electron donors such as MeOH as sacrificial agent in comparison [13,41-45] to their photocatalytic activity in pure water (overall water splitting).[20-21] In contrast to the controls and to our delight, UV-Vis irradiation of the MOFs in H_2O-CH_3OH solvent promoted in all cases the reduction of 4-nitrophenol to 4-aminophenol (Figure 2). The temporal evolution of the light-assisted, tandem reaction depended on the nature of the MOF. The most active bifunctional catalyst in this study, both under UV-Vis or simulated sunlight irradiation was UiO-66(Zr)-NH_2. An optimal amount of 5 mg of UiO-66(Zr)-NH_2 was determined for 1.25+1.25 mL H_2O-CH_3OH solution of p-nitrophenol (0.02 mmol) (Figure S14). Lower and higher catalyst amount either diminishes the number of active centers or increases the turbidity of the reaction medium hampering light penetration, respectively.

The higher efficiency of UiO-66(Zr)-NH_2 as bifunctional catalyst derives from its higher photocatalytic activity in H_2 generation under UV-Vis or simulated sunlight. This higher photocatalytic activity of UiO-66(Zr)-NH_2 respect to UiO-66(Zr)-H and UiO-66(Zr)-NO_2 can be explained as a combination of enhanced visible-light absorption and its more negative lower unoccupied crystal orbital (LUCO) potential favouring H^+ reduction (Figure 4).[46-47] The higher photoactivity of UiO-66(Zr)-NH_2 respect to MIL-125(Ti)-NH_2 can be also explained considering the lower LUCO value of the former (Figure 4). [46-47] Independent measurements of photocatalytic H_2 evolution in H_2O-CH_3OH in the absence of 4-nitrophenol showed that the photocatalytic H_2 production by UiO-66(Zr)-NH_2 (15.5 mmol g-1 h-1) is higher than by MIL-125(Ti)-NH_2 (< 5 mmol g-1 h-1) upon UV-Vis irradiation for 5 h. These values agree with the relative activity order in the tandem p-nitrophenol reduction to p-aminophenol observed for UiO-66(Zr)-NH_2 respect to MIL-125(Ti)-NH_2, both having amino substituents.

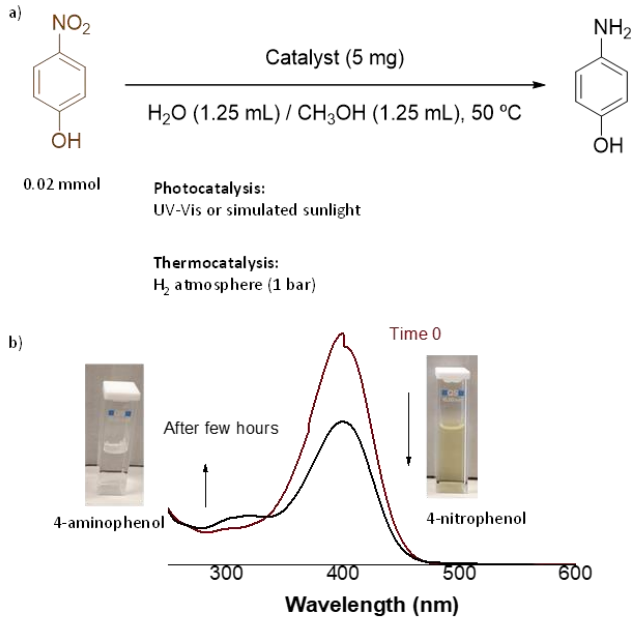

Figure 2. a) Photocatalytic or thermocatalytic 4-nitrophenol reduction to 4-aminophenol using MOFs. b) Changes in the transmission UV-vis absorption spectrum upon irradiation of 4-nitrophenol in water-methanol in the presence of MIL-125(Ti)-NH_2. The insets correspond to photographs of the cuvette before and after irradiation showing the variation of the visual appearance.

The variation in the relative activity order upon simulated solar light irradiation in favour of UiO-66(Zr)-NO_2 respect to UiO-66(Zr)-H is due to the enhanced visible light absorption of UiO-66(Zr)-NO_2 derived from the presence of the NO_2 group (Figure 2).

The photocatalytic reaction of p-nitrophenol to 4-aminophenol using methanol as hydrogen carrier is a tandem reaction that occurs in two steps. The first step is the photocatalytic hydrogen generation upon MOF photoexcitation using methanol as electron donor. Subsequently, H_2 should be activated by the MOFs. To study this step, additional experiments of 4-nitrophenol reduction were carried out in the dark using H_2 as reagent at 50 ºC. Figure 5 shows the relative catalytic activity of the series of the five MOF samples on the thermocatalytic 4-nitrophenol reduction to 4-aminophenol by H_2. Interestingly, all the MOFs exhibit catalytic hydrogenation activity, the most active MOF being the UiO-66(Zr)-NO_2, followed by UiO-66(Zr)-H and UiO-66(Zr)-NH_2.

This trend in activity follows the order of Lewis acid strength of metal nodes in UiO-66(Zr)-X (X: NO_2, H or NH_2) due to the inductive effect of substituents on terephthalate linker that has been previously observed in Lewis acid catalyzed reactions.[48] Thus, catalytic data indicate that the higher the Lewis acidity of the metal nodes, the higher the hydrogenating activity. It is likely that higher Lewis acid strength enhances H_2 polarization and, therefore, activates molecular H_2 towards the formation of metal-hydride species responsible for the reduction of the 4-nitrophenol to 4-aminophenol.[49] Accordingly, it is proposed that frustrated Lewis acid-base pairs in UiO-66(Zr)-X (X: NO_2, H or NH_2) are the sites to activate H_2 molecule forming a metal hydride and protonating basic sites.

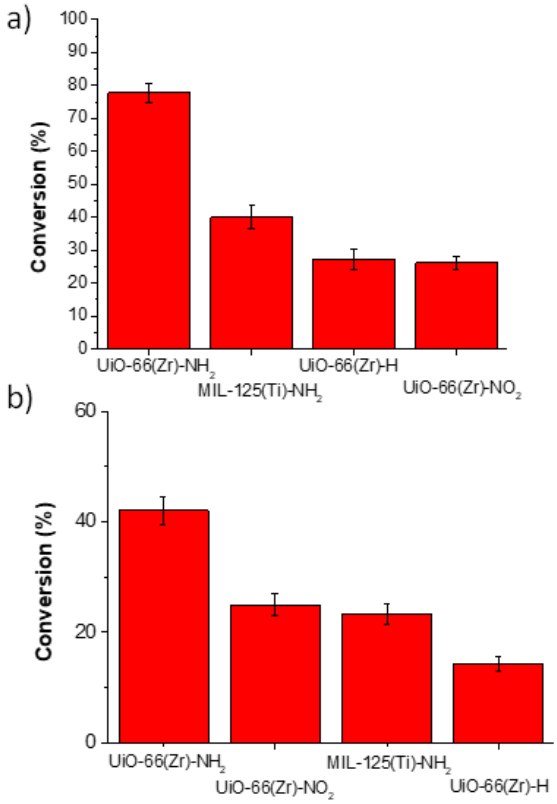

Figure 3. Light-assisted 4-nitrophenol hydrogenation to 4-aminophenol using methanol as hydrogen source under UV-Vis irradiation from a Xe lamp (a) or simulated sunlight irradiation (b) using MOFs. Reaction conditions: Catalyst (5 mg), p-nitrophenol (0.02 mmol), solvent (H_2O:MeOH, 1.25:1.25 mL), photoreactor volume (51 mL), Xe lamp (150 W) with or without 1.5AM filter, 50 °C.

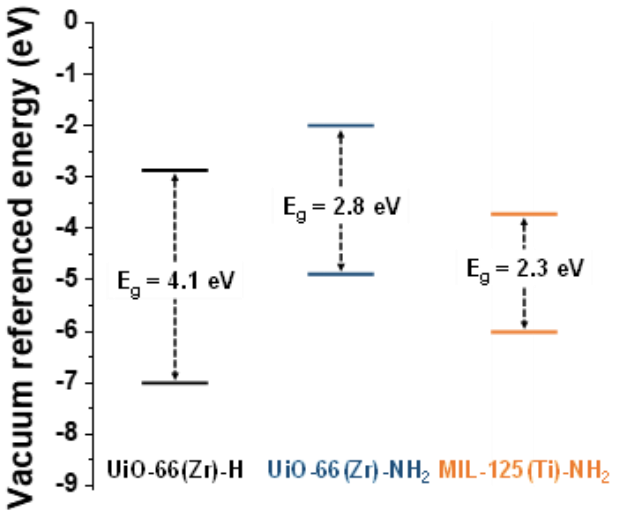

Figure 4. Energy band positions for MIL-125(Ti)-NH_2, UiO-66(Zr) and UiO-66(Zr)-NH_2

According to the relative reaction rates, it appears that photocatalytic H_2 evolution is the slowest elementary reaction controlling the overall efficiency of the bifunctional catalysts.

The most active UiO-66(Zr)-NH_2 sample for the light-assisted reduction of 4-nitrophenol to 4-aminophenol was reused several times without significant decrease of activity and maintaining its crystallinity as revealed by PXRD (Figure 6). Importantly, if the photocatalyst is removed once the reaction has started and the system allowed reacting further under the same reaction conditions, but in the absence of any solid, 4-nitrophenol conversion stops. This observation indicates that the process is heterogeneous, ruling out thempty e contribution of leached species to the tandem reaction. The BET surface area values of the tested MOFs after catalysis, calculated from the N_2 isotherms and summarized in table S2, indicated that no significant changes have occurred in the surface of MIL-125(Ti)-NH_2 MOF the during the catalytic process. The decrease in the surface area for the UiO-66(Zr) series MOFs after catalysis could be attributed to the adsorption of the methanol oxidation products.

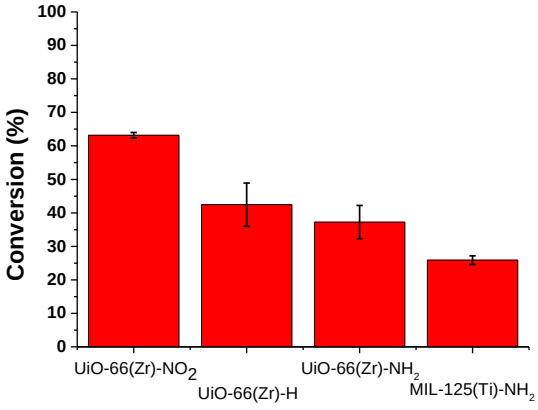

Figure 5. Catalytic hydrogenation of 4-nitrophenol to 4-aminophenol by molecular H_2 promoted by MOFs. Reaction conditions: Catalyst (5 mg), p-nitrophenol (0.02 mmol), solvent (H_2O:MeOH, 1.25:1.25 mL), reactor volume (51 mL), temperature 50 °C.

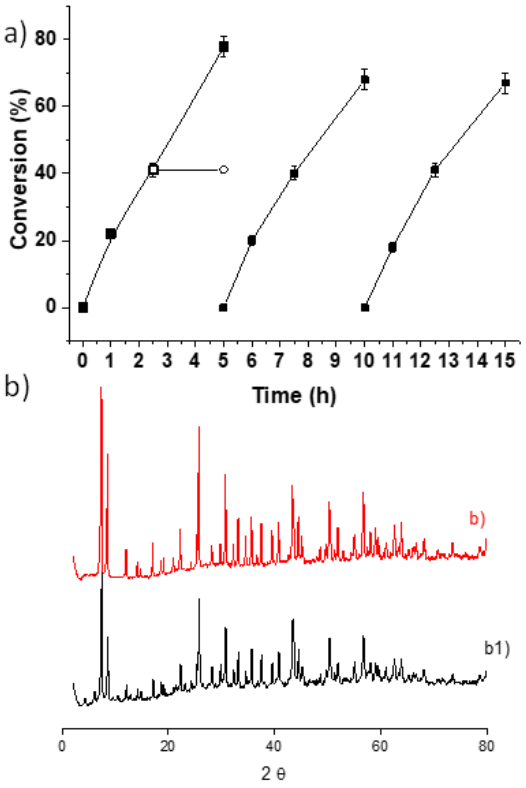

Figure 6. a) Reusability of UiO-66(Zr)-NH_2 as solid catalyst for the UV-Vis light-assisted reduction of 4-nitrophenol to 4-aminophenol by methanol as hydrogen source. The empty circle in the first run corresponds to an independent experiment in which the catalyst was filtered off at 2 h. b) Comparison of the PXRD patterns of fresh (b1) and three-times used (b2) UiO-66/(Zr)-NH_2 sample. Reaction conditions: Catalyst (5 mg), p-nitrophenol (0.02 mmol), solvent (H_2O:MeOH, 1.25:1.25 mL), photoreactor volume (51 mL), Xe lamp (150 W), 50 °C.

Conclusions

It has been shown that MOFs can promote hydrogenation of p-nitrophenol using methanol as hydrogen source. The tandem process requires light to promote the photocatalytic hydrogen generation, followed by frustrated Lewis acid-base pair activation of molecular hydrogen. It has been found that while H_2 activation is enhanced by electron withdrawing substituents, the controlling step in the tandem reaction is the light-assisted hydrogen generation from methanol. Accordingly, the most efficient catalysts found was UiO-66(Zr)-NH_2 that combines a more negative LUCO reduction potential and enhanced visible light absorption due to the bathochromic influence of the amino substituent. UiO-66(Zr)-NH_2 was stable under reaction conditions and can be reused without observing loss of its catalytic activity. The present study shows the potential of photocatalytic H_2 generation under favorable conditions to perform hydrogenation of organic compounds in

the absence of molecular H_2 by developing a tandem process, requiring frustrated Lewis acid-base pairs.

Conflicts of interest

"There are no conflicts to declare".

Acknowledgements

S.N. thanks financial support by the Fundación Ramón Areces (XVIII Concurso Nacional para la Adjudicación de Ayudas a la Investigación en Ciencias de la Vida y de la Materia, 2016), Ministerio de Ciencia, Innovación y Universidades RTI 2018-099482-A-I00 project and Generalitat Valenciana grupos de investigación consolidables 2019 (ref: AICO/2019/214) project. Financial support by the Spanish Ministry of Economy and Competitiveness (Severo Ochoa and RTI2018-098237-B-C21) and Generalitat Valenciana (Prometeo 2017-083) is also gratefully acknowledged.

Notes and references

1 T. Devic, C. Serre, *Chem. Soc. Rev.*, 2014, **43**, 6097–6115.
2 G. Férey, *Chem. Soc. Rev.*, 2008, **37**, 191–214.
3 S. Kitagawa, R. Kitaura, S.-I. Noro, *Angew. Chem., Int. Ed.*, 2004, **43**, 2334–2337.
4 H. Furukawa, K.E. Cordova, M. O'Keeffe, O.M. Yaghi, *Science*, 2013, **341**, 1230444.
5 H. García, S. Navalón, Metal-Organic Frameworks:Applications in Separations and Catalysis, Wiley, ISBN: 978-3-527-80910-3, 2018.
6 S.M. Cohen, *Chem. Sci.*, 2010, **1**, 32–36.
7 F. Vermoortele, M. Vandichel, B.V. de Voorde, R. Ameloot, M. Waroquier, V. Van Speybroeck, D.E. De Vos, *Angew. Chem. Int. Ed.*, 2012, **51**, 4887–4890.
8 A. Santiago-Portillo, J.F. Blandez, S. Navalón, M. Álvaro, H. García, *Catal. Sci. Technol.*, 2017, **7**, 1351–1362.
9 A. Santiago-Portillo, S. Navalón, P. Concepción, M. Álvaro, H. García, *ChemCatChem*, 2017, **9**, 2506–2511.
10 A. Dhakshinamoorthy, A. Santiago-Portillo, A.M. Asiri, H. Garcia, *ChemCatChem*, 2019, **11**, 899-923.
11 R. Zou, P.-Z. Li, Y.-F. Zeng, J. Liu, R. Zhao, H. Duan, Z. Luo, J.-G. Wang, R. Zou, Y. Zhao, *Small*, 2016, **12**, 2334–2343.
12 Q. Sun, M. Liu, K. Li, Y. Han, Y. Zuo, F. Chai, C. Song, G. Zhang, X. Guo, *Inorg. Chem. Front*., 2017, **4**, 144–153.
13 A. Dhakshinamoorthy, A.M. Asiri, H. García, *Angew. Chem. Int. Ed.*, 2016, **55**,5414-5445.
14 J. Tu, X. Zeng, F. Xu, X. Wu, Y. Tian, X. Hou, L. Long, *Chem. Commun.*, 2017, **53**, 3361–3364.
15 S.-N. Zhao, G. Wang, D. Poelman, P. Van Der Voort, *Molecules*, 2018, **23**, 2947.
16 Sun, D., Ye, L., Li, Z. *Applied Catalysis B: Environmental*, 2015, **164**, 428-432.
17 A. Santiago-Portillo, H. G. Baldoví, E. Carbonell, S. Navalón, M. Álvaro, H. García, B. Ferrer, *J. Phys. Chem. C*, 2018, **122**, 51, 29190–29199.
18 H. Luo, Z. Zeng, G. Zeng, C. Zhang, R. Xiao, D. Huang, C. Lai, M. Cheng, W. Wang, W. Xiong, Y. Yang, L. Qin, C. Zhou, H. Wang, Y. Zhou, S. Tian, *Chem. Eng. J.,* 2019, 123196.
19 Y. Shi, A.-F. Yang, C.-S. Cao, B. Zhao, *Coord. Chem. Rev.,* 2019, **390**, 50-75
20 S. Remiro-Buenamañana, M. Cabrero-Antonino, M. Martínez-Guanter, M. Álvaro, S. Navalón, H. García. *Applied Catalysis B: Environmental*, 2019, **254**, 677-684.
21 A. Melillo, M. Cabrero-Antonino, S. Navalón, M. Álvaro, B. Ferrer, H. García, *Applied Catalysis B: Environmental,* 2020, **278**, 1193452.
22 Y. Lee, S. Kim, J.K. Kang, S.M. Cohen, *Chem. Commun.*, 2015, **51**, 5735–5738.
23 I.I. Alkhatib, C. Garlisi, M. Pagliaro, K. Al-Ali, G. Palmisano, *Catal. Today*, 2020, **340**, 209-224.
24 R. Li, W. Zhang, K. Zhou, *Adv. Mater*., 2018, **30**, 1705512.
25 X. Pan, H. Xu, X. Zhao, H. Zhang, *ACS Sustainable Chem. Eng.*, 2020, **8**, 1087−1094.
26 H. Zhang, H. Xu, Y. Li, Y. Su, *Applied Materials Today*, 2020, **19**, 100609.
27 J. Wang, H. Xu, Ch. Ao, X. Pan, X. Luo, S. Wei, Z. Li, L. Zhang, Z. Xu, Y. Li, *iScience*, 2020, **23**, 101233.
28 Y.-B. Huang, J. Liang, X.-S. Wang, R. Cao, *Chem. Soc. Rev.*, 2017, **46**, 126–157.
29 C. Vallés-García, A. Santiago-Portillo, M. Álvaro, S. Navalón, H. García, *Applied Catalysis A: General,* 2020, **590**, 117340.
30 X. Liao, W. Wei, Y. Zhou, M. Zhang, Y. Cai, H. Liu, Y. Yao, S. Lu, Q. Haoa, *Catalysis Science and Technology,* 2020, **10**, 1015-1022.
31 Y. Hu, J. Zhang, H. Huo, Z. Wang, X. Xu, Y. Yang, K. Lin, R. Fan, *Catalysis Science and Technology*, 2020, **10**, 315-322.
32 D. Wang, Z. Li, *Catalysis Science and Technology,* 2015, **5,** 1623-1628.
33 Y. Wang, S. Yuan, K. Y. Wang, J. L. Li, G. S. Day, D. Qiu, L. Cheng, W.M. Chen, S. T. Madrahimov, H. C. Zhou, *ACS Catal.*, 2019, **9**, 6, 5111–5118.
34 A. Santiago Portillo, S. Navalón, M. Álvaro, H. García, *J. Catal.*, 2018, **365**, 450-463.
35 J. F. Blandez, A. Santiago-Portillo, S. Navalón, M. Giménez-Marqués, M. Álvaro, P. Horcajada, H. García, *Journal of Molecular Catalysis A: Chemical,* 2016, **425**, 332–33.
36 M.A. Nasalevich, R. Becker, E.V. Ramos-Fernandez, S. Castellanos, S.L. Veber, M.V. Fedin, F. Kapteijn, J.N.H. Reek, J.I. van der Vlugt, J. Gascon, *Energy Environ. Sci*., 2015, **8**, 364-375.
37 L. Shen, R. Liang, M. Luo, F. Jing, L. Wu, Phys. Chem. Chem. Phys, 2015, **17**, 117–121.
38 M. Kandiah, M.H. Nilsen, S. Usseglio, S. Jakobsen, U. Olsbye, M. Tilset, C.Larabi, E.A. Quadrelli, F. Bonino, K.P. Lillerud, *Chem. Mater.*, 2010, **24**, 6632–6640.
39 D. Cunha, C. Gaudin, I. Colinet, P. Horcajada, G. Maurin, C. Serre, *J. Mater. Chem. B*, 2013, **1**, 1101–1108.
40 J. Qiu, X. Zhang, Y. Feng, X. Zhang, H. Wang, *Applied Catalysis B: Environmental*, 2018, **231**, 317-342.
41 C.G. Silva, I. Luz, F. X. Llabrés I Xamena, A. Corma, H. García, *Chemistry - A European Journal*, 2010, **16**, 11133-11138.
42 B. Yan, L. Zhang, Z. Tang, M. Al-Mamum, H. Zhao, X. Su, *Applied Catalysis B: Environmental*, 2017, **218**, 743-750.
43 B. Zhang, J. Zhang, X. Tan, D. Shao, J. Shi, L. Zheng, J. Zhang, G. Yang, B. Han, *ACS Applied Materials and Interfaces,* 2018, **10**, 16418-16423.
44 I. Majeed, M. A. Nadeem, A. Badshah, F. K. Kanodarwala, H. Ali, M. A. Khan, J. A. Stride, M. A. Nadeem, *Catalysis Science and Technology*, 2017, **7**, 677-686.
45 Y. Shi, A.-F. Yang, C.-S. Cao, B. Zhao, *Coord. Chem. Rev.,* 2019, 390, 50-75.
46 J. G. Santaclara, A. I. Olivos-Suarez, A. Gonzalez-Nelson, D. Osadchii, M. A. Nasalevich, M. A. van der VeenO, F. Kapteijn, A. M. Sheveleva, S. L. Veber, M. V. Fedin, A. T. Murray, C. H. Hendon, A. Walsh, J. Gascon, *Chem. Mater.*, 2017, **29**, 21, 8963–8967

47 M.A. Nasalevich, C.H. Hendon, J.G. Santaclara, K. Svane, B. van der Linden, S.L. Veber, M. Fedin, A.J. Houtepen, M.A. van der Veen, F. Kapteijn, A. Walsh, J. Gascon, *Sci. Rep*., 2016, **6**, 23676.
48 A. Santiago-Portillo, S. Navalón, P. Concepción, M. Álvaro, H. García, *ChemCatChem*, 2017, **9**, 2506-2511
49 A. Kabadagi, S. Chikkamath, S. Kobayashi, J. Manjanna, *Applied Clay Science*, 2020, **189**, 105518.